

# uGMRT search for cold gas at $z \sim 1 - 1.4$ towards red quasars

R. Dutta<sup>1</sup> , R. Srianand<sup>2</sup>, N. Gupta<sup>2</sup>, R. Joshi<sup>3</sup>

<sup>1</sup> European Southern Observatory, Karl-Schwarzschild-Str. 2, D-85748 Garching Near Munich, Germany

<sup>2</sup> Inter-University Centre for Astronomy and Astrophysics, Post Bag 4, Ganeshkhind, Pune 411007, India

<sup>3</sup> Kavli Institute for Astronomy and Astrophysics, Peking University, Beijing 100871, People's Republic of China

Accepted. Received; in original form

## ABSTRACT

We present results from our search for H<sub>I</sub> 21-cm and OH 18-cm absorption at  $z \sim 1 - 1.4$  towards red quasars showing strong Mg II absorption using uGMRT. The quasars J1501+1822 and J1521+5508 show multiple strong associated Mg II absorption at  $z \sim 1.1$  and signature of reddening in their optical spectra. We report the detection of H<sub>I</sub> 21-cm absorption towards J1521+5508 at the systemic redshift of the quasar, with  $N(\text{H}_\text{I}) = (1.2 \pm 0.2) \times 10^{20} \text{ cm}^{-2}$  for spin temperature of 100 K and unit covering factor. The H<sub>I</sub> 21-cm absorption is offset from the blueshifted strong Mg II absorbers by  $\gtrsim 1500 \text{ km s}^{-1}$ . We do not detect H<sub>I</sub> 21-cm absorption at the redshift of the associated Mg II absorption and at the systemic redshift towards J1501+1822. We argue that lack of one-to-one correspondence between Mg II and H<sub>I</sub> 21-cm absorption could be related with clumpiness of the neutral gas and the radio and optical sightlines probing different volume of the gas. We find that the presence of strong associated Mg II absorption and reddening in the optical spectra of the quasars lead to an increased detection rate of associated H<sub>I</sub> 21-cm absorption at  $z \gtrsim 1$ . We also report non-detection of intervening OH absorption ( $[\text{OH}]/[\text{H}_\text{I}] \leq (1.4) \times 10^{-8}$ ) at  $z = 1.3$  towards two red quasars, J0850+5159 and J0852+3435, which show strong metal and H<sub>I</sub> 21-cm absorption and the 2175 Å dust extinction bump.

**Key words:** galaxies: quasar: absorption line – galaxies: ISM

## 1 INTRODUCTION

H<sub>I</sub> 21-cm absorption towards radio-loud quasars can be used to probe the cold neutral gas in intervening galaxies, usually selected via the presence of Lyman –  $\alpha$  or Mg II absorption in the quasar's optical spectra (e.g. Briggs & Wolfe 1983; Lane 2000; Curran 2010; Kanekar et al. 2009, 2014; Gupta et al. 2009, 2012; Srianand et al. 2012; Dutta et al. 2017a,b,c). The average detection rate of H<sub>I</sub> 21-cm absorption in strong Mg II systems is  $\sim 20\%$  over  $0.5 < z < 1.5$ , and has been found to increase with equivalent width of Mg II and Fe II absorption (Gupta et al. 2012; Dutta et al. 2017b), while the detection rate in  $2 < z < 3$  damped Lyman –  $\alpha$  absorbers is  $\sim 10\text{--}20\%$  (Srianand et al. 2012; Kanekar et al. 2014). The neutral gas in the environment of radio-loud active galactic nuclei (AGNs) can be probed by H<sub>I</sub> 21-cm absorption as well (e.g. van Gorkom et al. 1989; Gupta et al. 2006; Chandola et al. 2011; Curran et al. 2013; Allison et al. 2014; Geréb et al. 2015; Maccagni et al.

2017; Aditya & Kanekar 2018a,b; Dutta et al. 2018, 2019; Grasha et al. 2019). Such studies find a typical detection rate of  $\sim 30\%$  in  $z < 1$  radio galaxies. However, searches for H<sub>I</sub> 21-cm absorption associated to  $z > 1$  AGNs have been mostly unsuccessful ( $\leq 10\%$  detection rate). This could reflect either a lack of neutral gas along the line of sight due to geometric effects (e.g. Gupta et al. 2006) or stronger ionization by the high- $z$  AGNs compared to the low- $z$  samples (e.g. Curran et al. 2008; Grasha et al. 2019).

Complementary to H<sub>I</sub> 21-cm absorption, OH 18-cm absorption lines can be used to study the cold molecular phase of the gas. The OH radical is one of the common constituents of diffuse and dense molecular clouds and one of the best tracers of molecular hydrogen in the Galaxy (Liszt & Lucas 1996, 1999). In addition, the H<sub>I</sub> 21-cm and OH 18-cm absorption lines, if detected at high significance level, can be used to place tight constraints on the variations of fundamental constants of physics (Uzan 2003). However, only six OH absorbers at cosmologically significant redshifts in radio wavelengths are known to date (Chengalur et al. 1999;

\* E-mail: rdupta@eso.org

Chengalur & Kanekar 2003; Kanekar & Chengalur 2002; Kanekar et al. 2005; Gupta et al. 2018).

Quasars obscured by dust, either in intervening galaxies along the line-of-sight or in the quasar host galaxy itself, could present optimal sightlines to detect cold gas associated with the dust via H<sub>I</sub> and metal absorption. Such quasars could be identified on the basis of their red optical, infrared or optical-to-infrared colours and in radio-selected samples (Gregg et al. 2002; Ross et al. 2015; Glikman et al. 2018). We note, however, that the red colours of quasars could also arise due to their intrinsically red spectral energy distribution (SED), for example due to synchrotron emission from the radio jets (Srianand & Kembhavi 1997; Whiting et al. 2001).

There have been observations of H<sub>I</sub> 21-cm absorption arising from dusty intervening galaxies that cause reddening in the optical spectra of the background quasars (Srianand et al. 2008; Dutta et al. 2017b). In case of associated H<sub>I</sub> 21-cm absorption, Carilli et al. (1998) have found a high ( $\sim 80\%$ ) detection rate in a sample of five  $z \sim 0.7$  radio-selected optically-faint quasars (see also Ishwara-Chandra et al. 2003). Chandola & Saikia (2017) have found that  $z \leq 0.2$  radio galaxies with redder mid-infrared colours from Wide-field Infrared Survey Explorer (WISE; Wright et al. 2010) show a higher detection rate of H<sub>I</sub> 21-cm absorption. Further, Curran et al. (2006) have found that the molecular fraction and line strength of associated OH absorbers are related with the optical-to-infrared colour of the quasars.

However, there have also been studies that find low detection rates of associated H<sub>I</sub> 21-cm absorption in obscured quasars. Yan et al. (2016) have found a  $\sim 20\%$  detection rate in obscured AGNs at  $0.2 < z < 1.5$ , selected on basis of optical-to-near-infrared colours, although their results could be limited by presence of radio frequency interference (RFI) and absence of accurate spectroscopic redshifts. Recently, Glowacki et al. (2019) have found a detection rate of  $\sim 12.5\%$  ( $\sim 25\%$  for sources with spectroscopic redshifts) in a sample of  $0.4 < z < 1$  quasars selected on the basis of their radio flux and either faint optical magnitude or red WISE mid-infrared colour. All the three H<sub>I</sub> 21-cm absorption detected by them are from the sub-sample of optically-faint quasars. However, the lack of H<sub>I</sub> 21-cm absorption in their WISE mid-infrared colour-selected sub-sample is not statistically significant.

Here we explore an alternative method to select dust-obscured red quasars to search for H<sub>I</sub> 21-cm and OH 18-cm absorption – quasars showing optical reddening and strong Mg II absorption. One expects dust to be associated with metal-enriched gas, and  $E(B - V)$  or reddening of quasars has been found to depend on the equivalent width of strong Mg II absorption (Budzynski & Hewett 2011). Dutta et al. (2017b) have demonstrated that intervening H<sub>I</sub> 21-cm absorption arises on an average in systems with stronger metal absorption and towards quasars which show higher reddening [i.e.  $E(B - V)$ ] due to dust associated with the H<sub>I</sub> and metal absorption in their optical spectra. We investigate here whether red quasars showing strong associated Mg II absorption give rise to H<sub>I</sub> 21-cm absorption as well. According to hierarchical models of gas-rich major merger-driven galaxy formation, in the initial black hole growth phase fueled by gas inflow, the nuclear region is buried in

dust (Sanders & Mirabel 1996; Hopkins et al. 2008). Associated H<sub>I</sub> 21-cm absorption from red quasars is thus an useful tool to probe feedback processes in this dust-enshrouded phase of quasar evolution. Recently, we have obtained high detection rate ( $\sim 84\%$ ) of H<sub>I</sub> 21-cm absorption in  $z \leq 0.2$  radio-loud galaxy mergers (Dutta et al. 2018, 2019). Dust-reddened quasars can allow us to probe the merger phase at higher redshifts as well.

To address the paucity of H<sub>I</sub> 21-cm and OH 18-cm absorption at high- $z$ , we have started to search for these lines in previously unexplored redshift ranges towards  $z > 1$  red quasars, using the newly commissioned upgraded Giant Metrewave Radio Telescope (uGMRT; Gupta 2014) receivers. These receivers offer almost continuous frequency coverage over 120 – 1450 MHz, thus allowing one to search for absorption lines in redshift ranges that were not previously accessible to radio interferometers in relatively RFI-free environment, e.g. H<sub>I</sub> 21-cm at  $z \sim 0.7 - 1.2$  and OH 18-cm at  $z \sim 1 - 1.6$ . Such searches would be useful to plan future observations with the Square Kilometre Array precursors, ASKAP (Schinckel et al. 2012) and MeerKAT (Booth & Jonas 2012). Note that although the Green Bank Telescope currently offers broad frequency coverage below 1 GHz, it is a single dish and hence more affected by RFI. Here we present the results from our search for intervening OH 18-cm main absorption lines at  $z = 1.3$  towards the red quasars – J085042.24+515911.6 (hereafter J0850+5159) and J085244.74+343540.4 (hereafter J0852+3435); and our search for associated H<sub>I</sub> 21-cm absorption at  $z = 1.1$  towards the red quasars – J150129.87+182221.1 (hereafter J1501+1822) and J152134.17+550857.2 (hereafter J1521+5508). The details of the sources and observations are presented in Section 2. The results on individual sources are presented in Section 3. These are discussed and summarized in Section 4.

## 2 SAMPLE & OBSERVATIONS

### 2.1 Source Selection

#### 2.1.1 Sources for OH 18-cm absorption search

We selected J0850+5159 and J0852+3435 to search for OH 18-cm absorption because they both show strong H<sub>I</sub> 21-cm and metal absorption lines, dust reddening [ $E(B - V) \sim 0.3 - 0.4$ ] and the 2175 Å ultraviolet (UV) extinction bump (Srianand et al. 2008). Note that the broad absorption bump at 2175 Å is a spectroscopic feature due to extinction by interstellar dust, most likely polycyclic aromatic hydrocarbons, that is seen in the Milky Way, Magellanic Clouds, as well as high- $z$  absorption-line systems (Draine 2003; Wang et al. 2004; Jiang et al. 2011). Hence, while the reason for the reddening of the optical continuum of the quasar could be degenerate (see Section 1), the 2175 Å bump confirms the presence of dust unambiguously.

The above two quasars were part of a systematic survey of H<sub>I</sub> 21-cm absorption in  $z \sim 1.3$  strong Mg II systems (Gupta et al. 2009). Strong absorption from Mg II [rest equivalent width (REW) of Mg II  $\lambda 2796$ ,  $W_{\text{Mg II}} = 4.6$  Å and 2.9 Å for J0850+5159 and J0852+3435, respectively], Fe II (REW of Fe II  $\lambda 2600$ ,  $W_{\text{Fe II}} = 2.3$  Å and 2.1 Å for J0850+5159 and J0852+3435, respectively), as well as

weaker transitions of Mn II, Zn II, Cr II and Ti II, are detected at  $z = 1.3$  in the Sloan Digital Sky Survey (SDSS; [York et al. 2000](#)) spectra of the quasars. In addition, the  $9.7\mu\text{m}$  silicate feature is detected in absorption from the  $z = 1.3$  system towards J0852+3435 ([Kulkarni et al. 2011](#)). The background radio sources are relatively weak, with 1.4 GHz flux density of 63 mJy and 69 mJy for J0850+5159 and J0852+3435, respectively.

In the H I 21-cm absorption survey of  $z \sim 1.3$  strong Mg II systems, there is another system associated with a  $2175\text{\AA}$  bump towards the red quasar J095631.05+404628.2 (J0956+4046; [Gupta et al. 2012](#)). This system is very similar to J0850+5159 and J0852+3435 in terms of metal line strength and reddening properties. However, the background radio source in this case is resolved into two components in the GMRT 610 MHz image and no H I 21-cm absorption is detected towards it, leading to constraint on the spin temperature ( $T_s$ ) and covering factor ( $f_c^{\text{H}_1}$ ) of the gas,  $T_s/f_c^{\text{H}_1} > 7800\text{ K}$  (for details see section 5.2 of [Gupta et al. 2012](#)). Hence, we did not consider this system for OH 18-cm search.

### 2.1.2 Sources for H I 21-cm absorption search

We identified the red quasars, J1501+1822 and J1521+5508, from the SDSS Data Release 12 (DR12; [Alam et al. 2015](#)), specifically using the Mg II catalog of [Zhu & Ménard \(2013\)](#). We searched for strong Mg II absorption [ $W_{\text{Mg II}} \geq 1\text{\AA}$ ] whose redshifted H I 21-cm line can be observed with uGMRT, towards radio-loud quasars [1.4 GHz flux  $\geq 100\text{ mJy}$  in the Faint Images of the Radio Sky at Twenty-Centimeters (FIRST; [White et al. 1997](#)) catalog]. We restricted to sources where the optical and radio sightlines match within  $1''$  radius. We then selected those quasars which have  $r - i$  colour excess [ $\Delta(r - i)$ ] greater than  $3\sigma$  of the distribution, where  $\Delta(r - i)$  is calculated by comparing the  $r - i$  colour of the quasar to the median  $r - i$  colour for SDSS quasars at the same redshift. This led to a sample of fifteen red quasars. We visually inspected the optical spectra of these quasars, and after removing systems with false identification of Mg II or incorrect estimate of  $W_{\text{Mg II}}$ , Broad Absorption Line (BAL) quasars, and double radio sources (to avoid ambiguity between optical and radio sightlines), we were left with eight quasars. Five of them show intervening Mg II absorption over  $z \sim 0.6\text{--}2.0$  and three show associated (within  $\sim 3000\text{ km s}^{-1}$  of the systemic redshift) Mg II absorption at  $z \sim 1.1$ .

We fitted the quasar SDSS spectra by using the composite spectra of [Selsing et al. \(2016\)](#) and [Vanden Berk et al. \(2001\)](#), reddened by the Milky Way, Small Magellanic Cloud (SMC), Large Magellanic Cloud (LMC) or LMC2 supershell extinction curves ([Gordon et al. 2003](#)). Both the composite spectra give similar results. We assume that the reddening is caused due to dust present in the strong Mg II absorption. For details of the SED fitting procedure we refer to [Srianand et al. \(2008\)](#). The reddening of the quasars thus obtained is in the range of  $E(B - V) \sim 0.1\text{--}0.3$ , which is significant at  $\geq 2\sigma$  on comparing to control sample of quasars at the same redshift (see Section 3.2 for further details). Of the above eight quasars, six have been previously searched for H I 21-cm absorption at the redshift of the strong Mg II system, with two detections ([Ishwara-Chandra et al. 2003](#);

[Gupta et al. 2009](#); [Kanekar et al. 2009](#); [Dutta et al. 2017b](#))<sup>1</sup>. Results of the H I 21-cm absorption search towards the remaining two quasars, showing multiple strong associated Mg II absorption at  $z \sim 1.1$ , are presented in this work.

## 2.2 Observations

The radio spectral line searches were conducted using Band 4 (550–850 MHz) receivers of the uGMRT and the GMRT software back-end as the correlator (Proposal IDs: 32\_050, 33\_100, 34\_022, 34\_034). The details of the observations are listed in Table 1. The observations were carried out using 2, 4 or 16 MHz baseband bandwidth split into 512 channels. During the observations, standard calibrators were regularly observed for flux density, bandpass and gain calibration. The data were acquired in parallel hand correlations, and were reduced using the National Radio Astronomy Observatory (NRAO) Astronomical Image Processing System (AIPS) following standard procedures (see [Dutta et al. 2016](#), for details).

## 3 RESULTS

The results derived from the uGMRT observations are listed in Table 2. All the radio sources are compact in the continuum maps (spatial resolution of  $\sim 4\text{--}5''$ ). The absorption spectra (see Fig. 1) are extracted at the location of the peak continuum flux density of the radio sources. Below we discuss the results for each source in detail.

### 3.1 OH 18-cm absorption towards J0850+5159

[Srianand et al. \(2008\)](#) have modeled the SED of the quasar J0850+5159 using the SDSS composite spectrum of [Vanden Berk et al. \(2001\)](#) and different dust extinction curves redshifted to the rest-frame of the intervening Mg II absorption. The LMC2 supershell extinction curve is found to give best fit to the quasar SED, with  $E(B - V) \sim 0.3$ . The SED modeling and the  $A_V$  versus  $N(\text{H}_1)$  relationship in the LMC ([Gordon et al. 2003](#)) gives  $N(\text{H}_1) \sim 5 \times 10^{21} \kappa^{-1} \text{ cm}^{-2}$ , where  $\kappa$  is the dust-to-gas ratio relative to the LMC. The results from SED fitting are listed in Table 3. The H I 21-cm absorption consists of two components (full-width-at-half-maximum, FWHM =  $24\text{ km s}^{-1}$  and  $49\text{ km s}^{-1}$ ) separated by  $\sim 23\text{ km s}^{-1}$ , with an integrated optical depth of  $15\text{ km s}^{-1}$ .

We do not detect absorption from the two OH 18-cm main lines in this system (see panel (a) of Fig. 1). We reach a  $3\sigma$  optical depth limit for the  $1667\text{ MHz}$  line of  $0.224\text{ km s}^{-1}$  over a velocity width of  $5\text{ km s}^{-1}$ . This translates to a column density upper limit of  $N(\text{OH}) \leq 2 \times 10^{14} (\text{T}_{\text{ex}}/3.5\text{ K}) (1/f_c^{\text{OH}}) \text{ cm}^{-2}$ , where  $\text{T}_{\text{ex}}$  is the excitation temperature and  $f_c^{\text{OH}}$  is the covering factor (following [Liszt & Lucas 1996](#); [Stanimirović et al. 2003](#)).  $\text{T}_{\text{ex}} = 3.5\text{ K}$  is the peak of the

<sup>1</sup> One of the quasars, J092136.23+621552.1, showing intervening Mg II and H I 21-cm absorption ([Dutta et al. 2017b](#)), has been searched for and not detected in associated H I 21-cm absorption ([Aditya et al. 2016](#)). However, there is no associated Mg II absorption ( $W_{\text{Mg II}} \leq 1\text{\AA}$ ) detected in the SDSS spectrum as well.

**Table 1.** uGMRT observation log.

Quasar	$z_{\text{em}}$	$z_{\text{abs}}$	Date	Time (h)	Central Frequency (MHz)	Spectral coverage ( $\text{km s}^{-1}$ )	Channel width ( $\text{km s}^{-1}$ )
(1)	(2)	(3)	(4)	(5)	(6)	(7)	(8)
J0850+5159	1.894	1.3265	2017 July 02, 03	8.4	716.3	1745	3.4
J0852+3435	1.652	1.3095	2017 July 22, 23	25.7	721.5	1730	3.4
			2018 August 11, 13, 19				
J1501+1822	1.186	1.1859, 1.1818	2018 January 19	5.8	650.4	1920	3.8
J1521+5508	1.070	1.0450, 1.0593, 1.0654	2018 January 01	6.1	692.2	7200	14.1
			2018 August 12	5.3	686.1	910	1.8

*Notes.* Column 1: quasar name. Column 2: redshift of quasar. Column 3: redshift of strong Mg II absorption. Column 4: observation date. Column 5: total time on-source in hours. Column 6: central observing frequency in MHz. Column 7: spectral coverage in  $\text{km s}^{-1}$ . Column 8: channel width in  $\text{km s}^{-1}$ .

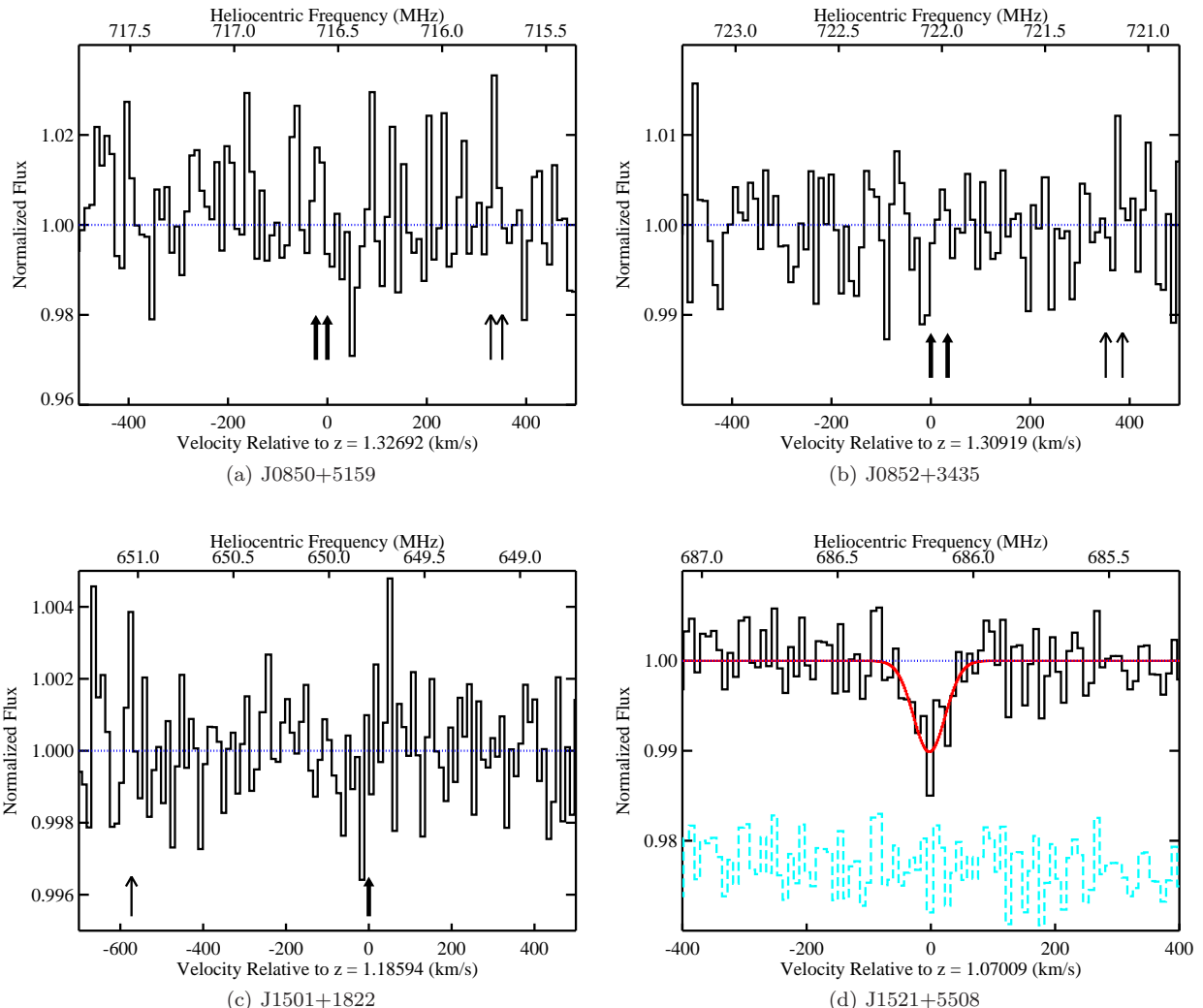


**Figure 1.** Absorption spectra towards the red quasars studied here. The spectra have been smoothed to  $10 \text{ km s}^{-1}$  for display purpose. (a) OH 18-cm absorption spectrum towards J0850+5159. The thick (thin) arrows indicate the expected positions of the redshifted 1667 MHz (1665 MHz) line from the H I 21-cm absorption components at  $z = 1.32692$  and  $z = 1.32674$ . (b) OH 18-cm absorption spectrum towards J0852+3435. The thick (thin) arrows indicate the expected positions of the redshifted 1667 MHz (1665 MHz) line from the H I 21-cm absorption components at  $z = 1.30919$  and  $z = 1.30945$ . (c) H I 21-cm absorption spectrum towards J1501+1822. The thick (thin) arrow indicates the expected position of the redshifted H I 21-cm line from the Mg II absorption at  $z = 1.18594$  ( $z = 1.18177$ ). (d) H I 21-cm absorption detected towards J1521+5508. The best-fitting Gaussian is overplotted in red solid line. The residual from the fit is shown in blue dashed line, shifted arbitrarily on the  $y$ -axis. The velocity scale is with respect to the systemic redshift of the quasar. As discussed in the text, no H I 21-cm absorption is detected at the redshifts of the Mg II absorption.

**Table 2.** Results from the radio spectral line observations.

Quasar	Peak Flux	Spectral rms	$\tau_p$	$\int \tau dv$
	(mJy)	(mJy beam $^{-1}$ )		(km s $^{-1}$ )
(1)	(2)	(3)	(4)	(5)
J0850+5159	65	1.1	$\leq 0.017$	$\leq 0.224$ (OH)
J0852+3435	58	0.4	$\leq 0.007$	$\leq 0.092$ (OH)
J1501+1822	243	0.7	$\leq 0.003$	$\leq 0.144$ (H I)
J1521+5508	195	1.0	$0.021 \pm 0.005$	$0.65 \pm 0.09$ (H I)

*Notes.* Column 1: quasar name. Column 2: peak flux density in mJy beam $^{-1}$ . Column 3: spectral rms in mJy beam $^{-1}$  per  $\sim 3$  km s $^{-1}$ . Column 4: peak optical depth in case of detection or  $1\sigma$  upper limit in case of non-detections. Column 5: integrated optical depth in case of detection or  $3\sigma$  upper limit in case of non-detections. Note that the  $\int \tau dv$  upper limits corresponding to the OH 1667 MHz line towards J0850+5159 and J0852+3435 have been estimated for velocity width of 5 km s $^{-1}$ , while the  $\int \tau dv$  upper limit for the H I 21-cm line towards J1501+1822 have been estimated for velocity width of 100 km s $^{-1}$ .

**Table 3.** Parameters obtained from SED fit to the quasars.

Quasar	Dust Model	$E(B - V)$	$N(\text{H I})$ $\times 1/\kappa 10^{21}$ (cm $^{-2}$ )	$(\kappa T_s)$ $\times 1/f_c^{\text{H I}}$ (K)
(1)	(2)	(3)	(4)	(5)
J0850+5159	LMC2	$0.27 \pm 0.01$	$5.2 \pm 1.0$	$191^{+139}_{-73}$
J0852+3435	LMC2	$0.36 \pm 0.01$	$7.0 \pm 1.3$	$534^{+257}_{-171}$
J1501+1822	SMC Bar	$0.24 \pm 0.01$	$8.7 \pm 1.0$	$\geq 3 \times 10^4$
J1521+5508	SMC Bar	$0.15 \pm 0.01$	$5.3 \pm 0.8$	$4473^{+1503}_{-1137}$

*Notes.* Column 1: quasar name. Column 2: Best-fitting dust extinction model. Column 3: Best-fitting  $E(B - V)$ . Column 4:  $N(\text{H I})$  in units of  $1/\kappa 10^{21}$  (cm $^{-2}$ ) obtained from the relation between  $N(\text{H I})$  and  $A_V$  (Gordon et al. 2003).  $\kappa$  is the dust-to-gas ratio relative to the best-fitting dust model. Column 5:  $(\kappa T_s)/f_c^{\text{H I}}$  (K) obtained by comparing the  $N(\text{H I})$  from SED fit with the observed H I 21-cm  $\int \tau dv$ . The SED fit parameters for J0850+5159 and J0852+3435 are taken from Srianand et al. (2008).

lognormal function fitted to the  $T_{\text{ex}}$  distribution of Galactic OH absorbers (Li et al. 2018). The radio source is compact in the Very Long Baseline Array (VLBA) 20-cm subarcsecond-scale map presented in Gupta et al. (2012), which recovers all the arcsecond-scale flux. Hence, we take  $f_c^{\text{OH}}$  to be unity. Using the  $N(\text{H I})$  obtained from SED fitting discussed above and assuming  $\kappa = 1$ , we can put a limit on the abundance ratio  $[\text{OH}]/[\text{H I}] \leq 4 \times 10^{-8}$ .

### 3.2 OH 18-cm absorption towards J0852+3435

The SED of the quasar J0852+3435, similar to J0850+5159, is best fit with LMC2 extinction curve and  $E(B - V) \sim 0.4$  (Srianand et al. 2008). The  $N(\text{H I})$  derived from SED modeling is  $\sim 7 \times 10^{21} \kappa^{-1} \text{ cm}^{-2}$ . The H I 21-cm absorption from the Mg II system comprises a narrow (FWHM = 23 km s $^{-1}$ ) and a broad (FWHM = 63 km s $^{-1}$ ) component, separated by  $\sim 34$  km s $^{-1}$ . The total optical depth of the absorption is 7 km s $^{-1}$ .

We initially detected a tentative absorption feature near the expected position of the redshifted OH 18-cm main lines from this system in 2017. Hence, we obtained deeper observations of this system in 2018 (see Table 1). We observed this system for a total of  $\sim 26$  h on-source, reaching a spectral rms of 0.4 mJy beam $^{-1}$  per 3 km s $^{-1}$  channel. However, we do not detect any significant absorption feature in the final spectrum. The spectrum shown in panel (b) of Fig. 1 is obtained by coadding the noise-weighted normalized spectra from the five different observing runs. The tentative absorption feature is not produced consistently in all the runs as well as in the two different polarizations. The initial tentative feature could have been due to narrow sporadic low-level RFI (at 721.5 MHz), that is not significant in the final coadded spectra, due to the Doppler shift caused by heliocentric motion of the Earth between the different observing runs.

The final spectrum has a  $3\sigma$  optical depth sensitivity for the 1667 MHz line of  $0.092$  km s $^{-1}$  over a velocity width of 5 km s $^{-1}$ . This corresponds to  $N(\text{OH}) \leq 1 \times 10^{14}$  (T $_{\text{ex}}/3.5$  K)  $(0.68/f_c^{\text{OH}})$  cm $^{-2}$ . We estimate  $f_c^{\text{OH}} = 0.68$  based on the ratio of the flux density of the strongest component of the radio source detected in the VLBA 20-cm map (Gupta et al. 2012) to its arcsecond-scale flux density. Assuming  $\kappa = 1$  and the  $N(\text{H I})$  estimated from SED fitting, we get  $[\text{OH}]/[\text{H I}] \leq 1 \times 10^{-8}$ .

### 3.3 H I 21-cm absorption towards J1501+1822

The SDSS spectrum of the quasar J1501+1822 is intriguing as it is devoid of any prominent broad emission lines. We identify the redshift of the quasar from [O II] emission line and associated Mg II absorption line as  $z_{\text{em}} = 1.1859 \pm 0.0007$ . There is a second Mg II absorption  $\sim 570$  km s $^{-1}$  blue-ward at  $z=1.18177$  (see panel (a) of Fig. 3). The Mg II  $\lambda 2796$  transition at  $z=1.18594$  is blended with the Mg II  $\lambda 2803$  transition at  $z=1.18177$ , leading to  $W_{\text{Mg II}} \leq 2.3$  Å. For the  $z=1.18177$  absorption,  $W_{\text{Mg II}} = 1.23 \pm 0.20$  Å. Weak Fe II absorption lines are also detected from these two systems, with  $W_{\text{Fe II}} = 0.28 \pm 0.15$  Å at  $z = 1.18177$  and  $W_{\text{Fe II}} = 0.65 \pm 0.14$  Å at  $z=1.18594$ . For both the systems, we get a  $3\sigma$  upper limit on REW of Mg I  $\leq 0.27$  Å. From integrating the [O II] emission line, we get [O II] luminosity of  $4.0 \pm 0.3 \times 10^{42}$  erg s $^{-1}$  (uncorrected for dust). Quasars with associated Mg II absorption have been found to show significant excess in [O II] emission, which could be due to either enhanced star formation in the quasar host or the AGN itself (Shen & Ménard 2012; Khare et al. 2014). If the [O II] emission in this case is caused by starburst, then the star formation rate (SFR), uncorrected for dust, would be  $27 \pm 2$  M $_{\odot}$  yr $^{-1}$  (following Kewley et al. 2004).

The SDSS spectrum of the quasar is best fit with the SMC Bar extinction law and  $E(B - V) = 0.24 \pm 0.01$ , assuming that the reddening is due to dust associated with the strong Mg II absorption at the systemic redshift (see Fig. 2). The error in  $E(B - V)$  include the uncertainties in the extinction law parameters. Note that there are no strong intervening metal line absorption at  $z \geq 0.4$  detected in the SDSS spectrum, so the reddening of the quasar is most likely due to the associated Mg II system. We further applied the same SED fitting procedure with SMC Bar extinction law to a control sample of non-BAL quasars in SDSS, within

$\Delta z = \pm 0.1$  of  $z_{\text{em}}$  and  $\Delta r_{\text{mag}} = \pm 0.5$  of  $r_{\text{mag}}$  (21) of the quasar and having spectra with signal-to-noise ratio  $\geq 10$ . The details of the control sample are given in Fig. 2. The standard deviation of the  $E(B - V)$  distribution of the control sample reflects the typical systematic error in the SED fitting procedure due to the dispersion of the non-reddened quasar SED. In this case, we find that the quasar is reddened at a significance level of  $\sim 6\sigma$ . The best-fitting SED is also found to be consistent with the Galaxy Evolution Explorer (GALEX) UV photometry (Fig. 2). Here for the UV part of the wavelength, we have taken the composite spectrum of Telfer et al. (2002). From the near-UV (NUV) flux, we obtain the luminosity as  $3 \times 10^{21} \text{ W Hz}^{-1}$ .

$\text{H}\alpha$  21-cm absorption is not detected from this quasar at the redshift of either  $\text{Mg II}$  absorption (see panel (c) of Fig. 1). From the observed optical depth limit, the  $3\sigma$  upper limit on  $N(\text{H}\alpha)$  is  $3 \times 10^{19} (\text{T}_s/100 \text{ K}) (1/f_c^{\text{H}\alpha}) \text{ cm}^{-2}$  per  $100 \text{ km s}^{-1}$  linewidth. On the other hand, from SED fitting we expect  $N(\text{H}\alpha) \sim 9 \times 10^{21} \kappa^{-1} \text{ cm}^{-2}$ . Here  $\kappa$  is the dust-to-gas ratio relative to the SMC. Comparing the two  $N(\text{H}\alpha)$  estimates, we can constrain  $(\kappa \text{ T}_s)/f_c^{\text{H}\alpha} \geq 3 \times 10^4 \text{ K}$ . The radio source is classified as a flat-spectrum radio source (Healey et al. 2007), with flux of 55 mJy at 8.4 GHz and 97 mJy at 4.8 GHz, and a spectral index of  $-0.46$  between 650 MHz and 4.8 GHz. Considering the flat spectral index, the radio emission is likely to be compact, but in the absence of high resolution images the covering factor is undetermined.

### 3.4 $\text{H}\alpha$ 21-cm absorption towards J1521+5508

The red quasar J1521+5508 shows broad emission lines in its SDSS spectrum at  $z_{\text{em}} = 1.0701 \pm 0.0004$ . This is an interesting quasar which has three blueshifted  $\text{Mg II}$  absorption at  $z = 1.04504$ , 1.05926 and 1.06540 (see panel (b) of Fig. 3). The  $\text{Mg II}$  absorption lines could be arising from strong outflows from the quasar or from an over-density of galaxies clustering around the quasar. The  $\text{Mg II} \lambda 2796$  transition at  $z=1.06540$  is blended with the  $\text{Mg II} \lambda 2803$  transition at  $z=1.05926$ . The  $W_{\text{Mg II}}$  for the three absorption systems at  $z = 1.04504$ , 1.05926 and 1.06540 are  $2.15 \pm 0.12 \text{ \AA}$ ,  $1.5 \pm 0.1 \text{ \AA}$  and  $\leq 2.3 \text{ \AA}$ , respectively. The corresponding  $W_{\text{Fe II}}$  for the three systems are  $\leq 0.37 \text{ \AA}$ ,  $0.70 \pm 0.11 \text{ \AA}$  and  $\leq 0.37 \text{ \AA}$ , respectively. The  $3\sigma$  upper limit on REW of  $\text{Mg I}$  is  $\leq 0.29 \text{ \AA}$  for all three systems. The  $[\text{O II}]$  emission line detected in the SDSS spectrum at  $z=1.07009$  gives a dust-uncorrected luminosity of  $1.6 \pm 0.3 \times 10^{42} \text{ erg s}^{-1}$ , and SFR of  $11 \pm 2 \text{ M}_\odot \text{ yr}^{-1}$  (following Kewley et al. 2004), if the emission is due to starburst in the host galaxy. The UV luminosity of this quasar, based on the GALEX NUV photometry, is  $7 \times 10^{21} \text{ W Hz}^{-1}$ . This quasar is also identified as a candidate  $\gamma$ -ray blazar of mixed class based on its WISE mid-infrared colours (D'Abrusco et al. 2014).

Performing SED fitting of the quasar SDSS spectrum, we find that both SMC Bar and SMC Wing extinction laws give best fit to the quasar, with  $E(B - V) = 0.15 \pm 0.01$  and  $0.20 \pm 0.01$ , respectively. However, the fit obtained from SMC Bar extinction law is more consistent with the GALEX UV photometry (see Fig. 2). Hence, we adopt this fit for the discussion here. Based on SED fitting to a control sample of SDSS quasars (similar to Section 3.3), the reddening of

this quasar is significant at  $2.5\sigma$  level. The  $N(\text{H}\alpha)$  derived from the SED fitting is  $\sim 5 \times 10^{21} \kappa^{-1} \text{ cm}^{-2}$ . Note that the reddening is assumed to be due to dust present in the quasar host galaxy. Some of the reddening could also be due to dust associated with the blueshifted  $\text{Mg II}$  absorption systems, in which case the above estimated  $E(B - V)$  and  $N(\text{H}\alpha)$  values would be upper limits. SED fits that assume reddening due to dust in the quasar host galaxy or in the  $\text{Mg II}$  systems have similar  $\chi^2$  values. Note that there are no intervening  $\text{Mg II}$  systems detected over  $0.4 \leq z \leq 1.0$  in the SDSS spectrum.

Initially we observed this quasar with a bandwidth of 16 MHz and a resolution of  $\sim 14 \text{ km s}^{-1}$ , which covered the  $\text{H}\alpha$  21-cm line at the redshift of the three  $\text{Mg II}$  systems and at the systemic redshift of the quasar. We did not detect any absorption at  $z = 1.05926$  and 1.06540, and the frequency ranges around  $z = 1.04504$  were affected by poor bandpass stability and RFI. From this spectrum, we put a  $3\sigma$  upper limit on  $N(\text{H}\alpha) \leq 5 \times 10^{19} (\text{T}_s/100 \text{ K}) (1/f_c^{\text{H}\alpha}) \text{ cm}^{-2}$  per  $100 \text{ km s}^{-1}$  near  $z = 1.05926$  and 1.06540. In addition, we detected a tentative absorption at the quasar systemic redshift of 1.07009.

We carried out follow-up observation of this system, with a 2 MHz band centred at the tentative detection and a resolution of  $\sim 2 \text{ km s}^{-1}$ . The resultant spectrum confirmed the detection, with the peak optical depth detected at  $\sim 4\sigma$  and the integrated optical depth at  $\sim 7\sigma$ . We show the absorption spectrum rebinned to  $10 \text{ km s}^{-1}$  resolution in panel (d) of Fig. 1. The  $\text{H}\alpha$  absorption coincides with the systemic redshift of the quasar and is redshifted by  $\sim 3628 \text{ km s}^{-1}$ ,  $\sim 1568 \text{ km s}^{-1}$  and  $\sim 679 \text{ km s}^{-1}$  from the three  $\text{Mg II}$  absorption systems. Note that we do not detect any strong  $\text{Mg II}$  absorption ( $W_{\text{Mg II}} \leq 0.6 \text{ \AA}$ ) at the redshift of the  $\text{H}\alpha$  absorption. The total optical depth of the absorption translates to  $N(\text{H}\alpha) = (1.2 \pm 0.2) \times 10^{20} (\text{T}_s/100 \text{ K}) (1/f_c^{\text{H}\alpha}) \text{ cm}^{-2}$ . We fitted a single component Gaussian to the absorption profile with a FWHM of  $60 \text{ km s}^{-1}$ . The velocity width which contains 90% of the optical depth is  $75 \text{ km s}^{-1}$ .

Combining the observed optical depth and the  $N(\text{H}\alpha)$  derived from SED fitting, gives us  $(\kappa \text{ T}_s)/f_c^{\text{H}\alpha} \sim 4500 \text{ K}$ . Based on the 4.85 GHz flux of 45 mJy (Gregory & Condon 1991) and the observed flux in our uGMRT data, we estimate a spectral index of  $-0.75$  for the radio source. Since no sub-arcsecond-scale image exists for this radio source,  $f_c^{\text{H}\alpha}$  cannot be constrained. The dust-to-gas ratio in this system could be higher than that observed in the SMC, i.e.  $\kappa$  could be greater than unity, as is possible in high- $z$  absorbers due to different grain chemistry or size (see Shaw et al. 2016; Noterdaeme et al. 2017; Dutta et al. 2017b; Rawlins et al. 2018). This is similar to what is inferred from the lack of  $\text{H}\alpha$  21-cm absorption towards the red quasar J0956+4046 (see Section 2.1.1 and Gupta et al. 2012). The above estimate on  $(\kappa \text{ T}_s)/f_c^{\text{H}\alpha}$  can thus be taken as an upper limit on  $\text{T}_s$ .

## 4 DISCUSSION

We have started searching for  $\text{H}\alpha$  21-cm and  $\text{OH}$  18-cm absorption lines at  $z \geq 1$  towards red quasars in the newly available frequency ranges offered by the uGMRT. We have presented here the results for our search for  $\text{OH}$  18-cm absorption from two intervening strong  $\text{Mg II}$  systems at  $z = 1.3$  and  $\text{H}\alpha$  21-cm absorption from two associated strong

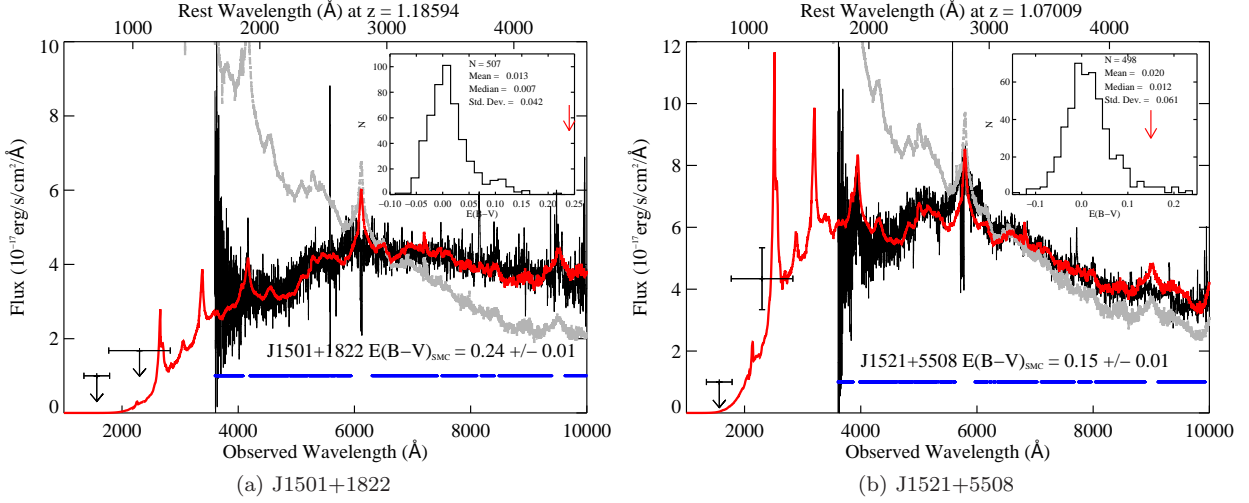


**Figure 2.** SED fit to the spectra of (a) J1501+1822 and (b) J1521+5508. The best-fitting SED (red), obtained from the SMC extinction curve, is overplotted on the SDSS spectrum (black) of the quasar in each panel. The non-reddened quasar composite spectrum (Selsing et al. 2016; Telfer et al. 2002) is shown in grey dashed lines. The points with error bars indicate the ultraviolet flux estimated from GALEX photometry. The horizontal lines indicate the spectral regions included in the fitting process. The best-fitting  $E(B - V)$  is indicated in each panel. The inset in each panel shows the distribution of  $E(B - V)$  for a control sample of SDSS quasars (see Section 3.3 for details), along with the number of quasars, mean, median and standard deviation of  $E(B - V)$  in the control sample. The arrows indicate the  $E(B - V)$  of the corresponding quasar.

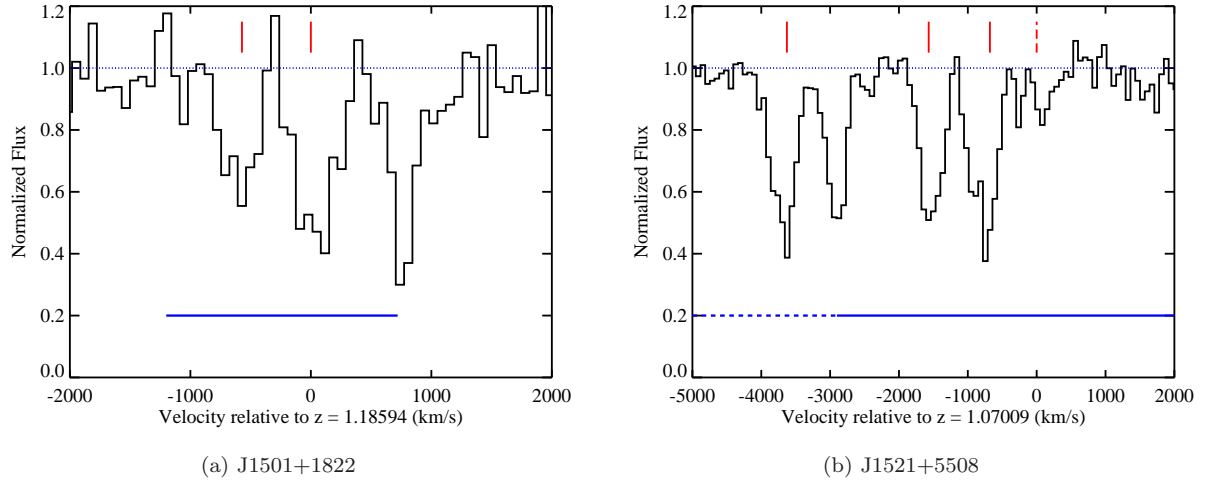


**Figure 3.** Normalized SDSS spectra of (a) J1501+1822 and (b) J1521+5508, showing the associated Mg II absorption at  $z \sim 1.1$ . The velocity scale is with respect to the  $z_{\text{em}}$  of the quasars. The solid vertical lines mark the position of the different Mg II  $\lambda 2796$  absorption lines. The dashed vertical line in panel (b) marks the redshift of the H I 21-cm absorption, which also coincides with the systemic redshift of the quasar. The solid horizontal lines demarcate the spectral coverage over which we have clean H I 21-cm absorption spectra. The dashed horizontal line demarcates spectral range affected by RFI.

Mg II systems at  $z = 1.1$ , all towards quasars showing reddening in their optical spectra [ $E(B - V) \sim 0.1 - 0.4$ ].

#### 4.1 OH 18-cm absorption towards red quasars

The quasars J0850+5159 and J0852+3435, although weak in their radio emission ( $\sim 60$  mJy at 1.4 GHz), were promising candidates for follow-up OH 18-cm absorption observations because of the presence of strong metal absorption ( $W_{\text{Mg II}} \gtrsim 3\text{\AA}$ ), 2175 Å extinction bump, and strong dust

reddening [ $E(B - V) \sim 0.3 - 0.4$ ]. The  $N(\text{H I})$  values [ $\sim (5 - 7) \times 10^{21} \text{ cm}^{-2}$ ] derived from SED fitting of the SDSS spectra are also high (Srianand et al. 2008), though there is no evidence for strong dependence of the OH detection rate on  $N(\text{H I})$  among the known Galactic and extragalactic OH absorbers (Gupta et al. 2018). The  $3\sigma$  upper limits achieved on  $N(\text{OH})$  [ $\sim (1 - 2) \times 10^{14} \text{ cm}^{-2}$ ] should be sensitive to detect the higher end of the  $N(\text{OH})$  detected in our Galaxy (Li et al. 2018; Rugel et al. 2018). The constraints on the  $[\text{OH}]/[\text{H I}]$  abundance ratio [ $\leq (1 - 4) \times 10^{-8}$ ] are lower than the median

$[\text{OH}]/[\text{H I}] \sim 10^{-7}$  observed in our Galaxy (Li et al. 2018; Rugel et al. 2018). This could indicate towards an evolution in the physical conditions and abundance of molecular gas at  $z > 1$ . However, we note that the scatter in the Galactic measurements is large, and that dust-to-gas ratios greater than that in the LMC would push the above derived limits higher. In both these systems, we can most likely rule out the presence of dense molecular gas. The presence of dust in these systems means that we cannot rule out the presence of molecular gas completely along these sightlines. We are hence probably still not reaching the sensitivity required to detect the diffuse molecular gas, i.e. with  $N(\text{OH}) \leq 10^{14} \text{ cm}^{-2}$ . The upcoming MeerKAT Absorption Line Survey (MALIS; Gupta et al. 2016) will specifically target bright high- $z$  quasars to reach OH column density sensitivities below this ( $\sim 5 \times 10^{13} \text{ cm}^{-2}$ ) over  $0 < z < 2$  (Gupta et al. 2018).

## 4.2 H I 21-cm absorption towards red quasars

We have detected H I 21-cm absorption at the systemic redshift of the quasar J1521+5508, with  $N(\text{H I}) = (1.2 \pm 0.2) \times 10^{20} \text{ (T}_s/100 \text{ K)} (1/f_c^{\text{H I}}) \text{ cm}^{-2}$ . However, we do not detect H I absorption from the blueshifted strong Mg II absorption systems along this line-of-sight [ $N(\text{H I}) \leq 5 \times 10^{19} \text{ (T}_s/100 \text{ K)} (1/f_c^{\text{H I}}) \text{ cm}^{-2}$ ]. We also do not detect H I absorption from the strong Mg II systems associated with the quasar J1501+1822 [ $N(\text{H I}) \leq 3 \times 10^{19} \text{ (T}_s/100 \text{ K)} (1/f_c^{\text{H I}}) \text{ cm}^{-2}$ ]. The reasons for non-detection of associated H I 21-cm absorption in general are the absence of neutral gas due to ionization by high luminosity-AGN, higher spin temperature in the vicinity of AGN, and extended background radio structure and small-scale structure in the absorbing gas itself leading to small covering factor. The two quasars discussed here show the presence of strong Mg II absorption and dust reddening, which indicate the presence of neutral gas in the vicinity of the quasars. The  $N(\text{H I})$  estimates inferred from SED fitting, assuming that the reddening is due to dust associated with the quasars, are  $\sim (5.9) \times 10^{21} \text{ cm}^{-2}$ . If part of the reddening is caused due to dust present in the blueshifted Mg II absorption systems, the  $N(\text{H I})$  estimates would be upper limits. Additionally, based on the  $W_{\text{Mg II}}$  and  $W_{\text{Fe II}}$ , the probability of  $N(\text{H I})$  being greater than  $10^{19}$  and  $10^{20} \text{ cm}^{-2}$ , is 92% and 51%, respectively (see Dutta et al. 2017b, for details). Further, the UV luminosity of these quasars is below the critical luminosity believed to ionize neutral gas completely (Curran et al. 2008; Curran & Whiting 2012). Hence, we can rule out the absence of neutral gas as the reason behind the lack of H I 21-cm absorption.

The relatively flat radio spectrum of these two quasars implies compact structure, though in absence of sub-arcsecond-scale images, the background radio structure and exact gas covering factor are uncertain. We are probing absorption over scales of  $\sim 30 - 40$  kpc at the redshift of the quasars<sup>2</sup>. It is likely that the neutral gas is present in small clumps along these sightlines, and we are not detecting H I 21-cm absorption from all the clumps due to difference in the

optical and radio sightlines. This would explain the detection of H I 21-cm absorption at the systemic redshift of the quasar J1521+5508 and non-detection at the redshift of the blueshifted Mg II absorption. Indeed, the absence of strong Mg II absorption at the redshift of the H I 21-cm absorption implies that the radio sightline is probing a different volume of gas than the optical sightline. Differences in H I 21-cm and metal absorption profiles, with the H I 21-cm absorption not always coinciding with the strongest metal component, have been observed even in intervening systems with high resolution optical spectra available (e.g. Gupta et al. 2009; Rahmani et al. 2012; Dutta et al. 2015). While no strong correlation has been found between line width of intervening H I 21-cm absorption and linear size of radio sources from subarcsecond-scale images, the largest velocity widths are seen towards radio sources with extended structure at arcsecond-scales (Gupta et al. 2012). This can be explained if the absorbing gas is patchy, which is consistent with the above scenario that gives rise to differences in H I and metal absorption.

Next, we discuss the detection rate of H I 21-cm absorption in red quasars and in particular the detection rate of associated absorption at  $z \geq 1$ . As outlined in Section 2.1.2, the two quasars, J1501+1822 and J1521+5508, were selected on the basis of their SDSS red colours and strong Mg II absorption. This selection procedure resulted in a total sample of eight red quasars (with associated and intervening absorbers), out of which six had been previously observed, with two detections. Hence, including the two quasars presented here, the detection rate of H I 21-cm absorption in this sample of red quasars is  $38_{-20}^{+36}\%$ <sup>3</sup>.

Considering only associated absorption, two out of three red quasars show H I 21-cm absorption — towards J1521+5508 reported here, and towards 3C 190 ( $z=1.2$ ) (Ishwara-Chandra et al. 2003). It is interesting to note that, similar to the velocity offset in H I and Mg II absorption towards J1521+5508, the peak H I optical depth in case of the absorption towards 3C 190 also does not coincide in velocity with the peak of the Mg II absorption. Even though the uncertainties are large due to the small number of red quasars searched to date at  $z \geq 1$ , the detection rate of associated H I 21-cm absorption in red quasars is higher than the typical detection rate ( $\leq 10\%$ ) in samples of  $z \geq 1$  AGNs selected without any condition on reddening or the presence of metal absorption. For example, from the compilation presented in Aditya & Kanekar (2018a) and Aditya & Kanekar (2018b), associated H I 21-cm absorption has been detected in 4 out of 56 flat-spectrum and gigahertz-peaked-spectrum radio sources at  $z \geq 1$ . SDSS spectrum is available for one of the four sources with detection (TXS 1200+045) and we do not detect any strong associated Mg II absorption ( $W_{\text{Mg II}} \leq 1 \text{ \AA}$ ) within  $\sim 3000 \text{ km s}^{-1}$  of the systemic redshift of the quasar. The optical spectra available for two other sources (TXS 1245-197 and TXS 1954+513) in the literature (di Serego Alighieri et al. 1994; Lawrence et al. 1996) do not show signature of associated Mg II absorption. However, these are very low-resolution ( $\sim 10 \text{ \AA}$ ) spectra from which we cannot place any strong constraints. Note that  $\sim 60\%$  of the H I absorption spectra reported in

<sup>2</sup> Adopting a flat  $\Lambda$ -cold dark matter cosmology with  $H_0 = 70 \text{ km s}^{-1} \text{ Mpc}^{-1}$  and  $\Omega_M = 0.30$ .

<sup>3</sup> Poissonian errors computed using tables of Gehrels (1986).

Aditya & Kanekar (2018a) and Aditya & Kanekar (2018b) are not sensitive enough to detect the absorption towards J1521+5508 reported here. For 17 of the sources with H<sub>I</sub> 21-cm non-detection, SDSS spectra are available, and we do not detect Mg II absorption ( $W_{\text{Mg II}} \leq 1 \text{ \AA}$ ) within  $\sim 3000 \text{ km s}^{-1}$  of the systemic redshift. Similarly, for the H<sub>I</sub> 21-cm non-detections in  $z \sim 1 - 2$  compact radio sources reported in the recent study of Grasha et al. (2019), no associated Mg II absorption is detected in the available SDSS spectra. Hence, the lack of H<sub>I</sub> 21-cm absorption in these cases is consistent with the absence of metal-rich neutral gas in the vicinity of the AGNs.

Next, we consider all quasars with associated Mg II absorption at  $z \geq 1$  in SDSS spectra that have been searched for H<sub>I</sub> 21-cm absorption. In addition to the three systems in our red quasar sample, there are five quasars that do not fulfill the optical colour or radio flux criteria of our sample (Section 2.1.2), but show Mg II absorption at  $\leq 3000 \text{ km s}^{-1}$  of the systemic redshift. Three out of these five have been detected in H<sub>I</sub> 21-cm absorption – J010826.84–003724.1 ( $z=1.375$ ; Gupta et al. 2009), J114521.32+045526.7 ( $z=1.345$ ; Kanekar et al. 2009), J091927.61+014603.0 ( $z=1.286$ ; Dutta et al. 2017b). The peak H<sub>I</sub> optical depth of the absorption is again offset (up to  $\sim 100 \text{ km s}^{-1}$ ) from the peak Mg II absorption in these systems. Two of these quasars have VLBA images available, which show structures in the radio emission at subarcsecond-scales, with  $f_c^{\text{H}_I} \sim 0.3\text{--}0.5$  (Gupta et al. 2012). This supports our above argument that the neutral gas near these AGNs have structures at small scales that give rise to different absorbing components in the optical and radio sightlines. The total detection rate of associated H<sub>I</sub> 21-cm absorption in the above Mg II-selected systems is  $62^{+0.38\%}_{-0.27\%}$  ( $57^{+0.43\%}_{-0.27\%}$  considering only  $W_{\text{Mg II}} \geq 1 \text{ \AA}$  systems). Thus, the presence of strong associated Mg II absorption increases the detection rate of associated H<sub>I</sub> 21-cm absorption in  $z \geq 1$  quasars. Due to small number statistics, we are not able to determine yet whether the presence of reddening signature further enhances the detection rate.

Similar to what has been found for intervening Mg II absorbers (Gupta et al. 2012; Dutta et al. 2017b), we do not find any correlation of the H<sub>I</sub> 21-cm optical depth and velocity width with  $W_{\text{Mg II}}$  of the associated Mg II absorption at  $z \geq 1$ , albeit the number of such absorbers is small (5). However, considering the effect of reddening alone, we find that the distributions of the colour excess,  $\Delta(r - i)$ , of the quasars with and without associated H<sub>I</sub> 21-cm absorption at  $z \geq 1$  are different. A two-sided Kolmogorov-Smirnov test gives maximum deviation between the two cumulative distributions as  $D_{\text{KS}} = 0.54$ , with the probability of finding this difference by chance being  $P_{\text{KS}} = 0.03$ . The effect of reddening due to dust can be seen more clearly from the geometric mean stacked SDSS spectra, at the rest-frame of the quasar, of the associated H<sub>I</sub> 21-cm absorbers (6) and non-absorbers (26) at  $z \geq 1$ <sup>4</sup> (Fig. 4). The quasars which show associated H<sub>I</sub> 21-cm absorption tend to be more reddened on average, with the stacked spectrum of quasars showing associated H<sub>I</sub> 21-

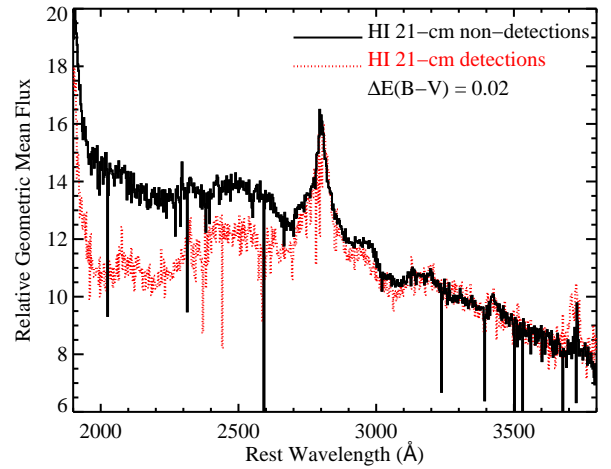


**Figure 4.** Stacked SDSS spectra (geometric mean) of the  $z \geq 1$  quasars at rest-frame, with and without detection of associated H<sub>I</sub> 21-cm absorption in red dotted and black solid lines, respectively.

cm absorption having a differential reddening of  $\Delta E(B - V) = 0.02$  with respect to the stacked spectrum of quasars not detected in associated H<sub>I</sub> 21-cm absorption. Therefore, there are indications of both strong Mg II absorption and optical reddening leading to higher occurrence of associated H<sub>I</sub> 21-cm absorption in  $z \geq 1$  quasars. Further searches towards reddened quasars along with characterization of the parsec-scale radio structure through VLBA imaging are the way forward towards understanding the incidence, distribution and physical conditions of neutral gas in high- $z$  quasars.

## ACKNOWLEDGEMENTS

We thank the anonymous reviewer for their helpful comments and suggestions. RD acknowledges support from the Alexander von Humboldt Foundation. We thank the staff at GMRT for their help during the observations. GMRT is run by the National Centre for Radio Astrophysics of the Tata Institute of Fundamental Research. Funding for SDSS-III has been provided by the Alfred P. Sloan Foundation, the Participating Institutions, the National Science Foundation, and the U.S. Department of Energy Office of Science. The SDSS-III web site is <http://www.sdss3.org/>. SDSS-III is managed by the Astrophysical Research Consortium for the Participating Institutions of the SDSS-III Collaboration including the University of Arizona, the Brazilian Participation Group, Brookhaven National Laboratory, Carnegie Mellon University, University of Florida, the French Participation Group, the German Participation Group, Harvard University, the Instituto de Astrofísica de Canarias, the Michigan State/Notre Dame/JINA Participation Group, Johns Hopkins University, Lawrence Berkeley National Laboratory, Max Planck Institute for Astrophysics, Max Planck Institute for Extraterrestrial Physics, New Mexico State University, New York University, Ohio State University, Pennsylvania State University, University of Portsmouth, Princeton University, the Spanish Participation Group, University of Tokyo, University of Utah, Vanderbilt University, University of Virginia, University of Washington, and Yale University.

<sup>4</sup> For this analysis we consider all the quasars searched for associated H<sub>I</sub> 21-cm absorption at  $z \geq 1$  that have SDSS spectra available.

## REFERENCES

Aditya J. N. H. S., Kanekar N., 2018a, *MNRAS*, **473**, 59

Aditya J. N. H. S., Kanekar N., 2018b, *MNRAS*, **481**, 1578

Aditya J. N. H. S., Kanekar N., Kurapati S., 2016, *MNRAS*, **455**, 4000

Alam S., et al., 2015, *ApJS*, **219**, 12

Allison J. R., Sadler E. M., Meekin A. M., 2014, *MNRAS*, **440**, 696

Booth R. S., Jonas J. L., 2012, *African Skies*, **16**, 101

Briggs F. H., Wolfe A. M., 1983, *ApJ*, **268**, 76

Budzynski J. M., Hewett P. C., 2011, *MNRAS*, **416**, 1871

Carilli C. L., Menten K. M., Reid M. J., Rupen M. P., Yun M. S., 1998, *ApJ*, **494**, 175

Chandola Y., Saikia D. J., 2017, *MNRAS*, **465**, 997

Chandola Y., Sirothia S. K., Saikia D. J., 2011, *MNRAS*, **418**, 1787

Chengalur J. N., Kanekar N., 2003, *Physical Review Letters*, **91**, 241302

Chengalur J. N., de Bruyn A. G., Narasimha D., 1999, *A&A*, **343**, L79

Curran S. J., 2010, *MNRAS*, **402**, 2657

Curran S. J., Whiting M. T., 2012, *ApJ*, **759**, 117

Curran S. J., Whiting M. T., Murphy M. T., Webb J. K., Longmore S. N., Pihlström Y. M., Athreya R., Blake C., 2006, *MNRAS*, **371**, 431

Curran S. J., Whiting M. T., Wiklind T., Webb J. K., Murphy M. T., Purcell C. R., 2008, *MNRAS*, **391**, 765

Curran S. J., Whiting M. T., Sadler E. M., Bignell C., 2013, *MNRAS*, **428**, 2053

D'Abrusco R., Massaro F., Paggi A., Smith H. A., Masetti N., Landoni M., Tosti G., 2014, *The Astrophysical Journal Supplement Series*, **215**, 14

Draine B. T., 2003, *ARA&A*, **41**, 241

Dutta R., Srianand R., Muzahid S., Gupta N., Momjian E., Charlton J., 2015, *MNRAS*, **448**, 3718

Dutta R., Gupta N., Srianand R., O'Meara J. M., 2016, *MNRAS*, **456**, 4209

Dutta R., Srianand R., Gupta N., Momjian E., Noterdaeme P., Petitjean P., Rahmani H., 2017a, *MNRAS*, **465**, 588

Dutta R., Srianand R., Gupta N., Joshi R., Petitjean P., Noterdaeme P., Ge J., Krogager J.-K., 2017b, *MNRAS*, **465**, 4249

Dutta R., Srianand R., Gupta N., Joshi R., 2017c, *MNRAS*, **468**, 1029

Dutta R., Srianand R., Gupta N., 2018, *MNRAS*, **480**, 947

Dutta R., Srianand R., Gupta N., 2019, *MNRAS*, **489**, 1099

Gehrels N., 1986, *ApJ*, **303**, 336

Geréb K., Maccagni F. M., Morganti R., Oosterloo T. A., 2015, *A&A*, **575**, A44

Glikman E., et al., 2018, *ApJ*, **861**, 37

Glowacki M., et al., 2019, *MNRAS*, p. 2114

Gordon K. D., Clayton G. C., Misselt K. A., Landolt A. U., Wolff M. J., 2003, *ApJ*

Grasha K., Darling J., Bolatto A., Leroy A. K., Stocke J. T., 2019, arXiv e-prints, p. arXiv:1909.12422

Gregg M. D., Lacy M., White R. L., Glikman E., Helfand D., Becker R. H., Brotherton M. S., 2002, *ApJ*, **564**, 133

Gregory P. C., Condon J. J., 1991, *The Astrophysical Journal Supplement Series*, **75**, 1011

Gupta Y., 2014, in *Astronomical Society of India Conference Series*. pp 441–447

Gupta N., Salter C. J., Saikia D. J., Ghosh T., Jeyakumar S., 2006, *MNRAS*, **373**, 972

Gupta N., Srianand R., Petitjean P., Noterdaeme P., Saikia D. J., 2009, *MNRAS*, **398**, 201

Gupta N., Srianand R., Petitjean P., Bergeron J., Noterdaeme P., Muzahid S., 2012, *A&A*, **544**, A21

Gupta N., et al., 2016, in *Proceedings of MeerKAT Science: On the Pathway to the SKA*. 25–27 May. p. 14

(arXiv:1708.07371)

Gupta N., Momjian E., Srianand R., Petitjean P., Noterdaeme P., Gyanchandani D., Sharma R., Kulkarni S., 2018, *ApJ*, **860**, L22

Healey S. E., Romani R. W., Taylor G. B., Sadler E. M., Ricci R., Murphy T., Ulvestad J. S., Winn J. N., 2007, *The Astrophysical Journal Supplement Series*, **171**, 61

Hopkins P. F., Hernquist L., Cox T. J., Kereš D., 2008, *ApJS*, **175**, 356

Ishwara-Chandra C. H., Dwarakanath K. S., Anantharamaiah K. R., 2003, *Journal of Astrophysics and Astronomy*, **24**, 37

Jiang P., Ge J., Zhou H., Wang J., Wang T., 2011, *ApJ*, **732**, 110

Kanekar N., Chengalur J. N., 2002, *A&A*, **381**, L73

Kanekar N., et al., 2005, *Physical Review Letters*, **95**, 261301

Kanekar N., Prochaska J. X., Ellison S. L., Chengalur J. N., 2009, *MNRAS*, **396**, 385

Kanekar N., et al., 2014, *MNRAS*, **438**, 2131

Kewley L. J., Geller M. J., Jansen R. A., 2004, *AJ*, **127**, 2002

Khare P., Berk Daniel V., Rahmani H., York D. G., 2014, *ApJ*, **794**, 66

Kulkarni V. P., Torres-Garcia L. M., Som D., York D. G., Welty D. E., Vladilo G., 2011, *ApJ*, **726**, 14

Lane W. M., 2000, PhD thesis, University of Groningen

Lawrence C. R., Zucker J. R., Readhead A. C. S., Unwin S. C., Pearson T. J., Xu W., 1996, *ApJS*, **107**, 541

Li D., et al., 2018, *ApJS*, **235**, 1

Liszt H., Lucas R., 1996, *A&A*, **314**, 917

Liszt H., Lucas R., 1999, in Carilli C. L., Radford S. J. E., Menten K. M., Langston G. I., eds, *Astronomical Society of the Pacific Conference Series Vol. 156, Highly Redshifted Radio Lines*. p. 188

Maccagni F. M., Morganti R., Oosterloo T. A., Geréb K., Maddox N., 2017, *A&A*, **604**, A43

Noterdaeme P., et al., 2017, *A&A*, **597**, A82

Rahmani H., Srianand R., Gupta N., Petitjean P., Noterdaeme P., Vásquez D. A., 2012, *MNRAS*, **425**, 556

Rawlins K., Srianand R., Shaw G., Rahmani H., Dutta R., Chacko S., 2018, *MNRAS*, **481**, 2083

Ross N. P., et al., 2015, *MNRAS*, **453**, 3932

Rugel M. R., et al., 2018, *A&A*, **618**, A159

Sanders D. B., Mirabel I. F., 1996, *ARA&A*, **34**, 749

Schinckel A. E., Bunton J. D., Cornwell T. J., Feain I., Hay S. G., 2012, in *Proc. SPIE*. p. 84442A, doi:10.1117/12.926959

Selsing J., Fynbo J. P. U., Christensen L., Krogager J.-K., 2016, *A&A*, **585**, A87

Shaw G., Rawlins K., Srianand R., 2016, *MNRAS*, **459**, 3234

Shen Y., Ménard B., 2012, *ApJ*, **748**, 131

Srianand R., Kembhavi A., 1997, *ApJ*, **478**, 70

Srianand R., Gupta N., Petitjean P., Noterdaeme P., Saikia D. J., 2008, *MNRAS*, **391**, L69

Srianand R., Gupta N., Petitjean P., Noterdaeme P., Ledoux C., Salter C. J., Saikia D. J., 2012, *MNRAS*, **421**, 651

Stanimirović S., Weisberg J. M., Dickey J. M., de la Fuente A., Devine K., Hedden A., Anderson S. B., 2003, *ApJ*, **592**, 953

Telfer R. C., Zheng W., Kriss G. A., Davidsen A. F., 2002, *ApJ*, **565**, 773

Uzan J.-P., 2003, *Reviews of Modern Physics*, **75**, 403

Vanden Berk D. E., et al., 2001, *AJ*, **122**, 549

Wang J., Hall P. B., Ge J., Li A., Schneider D. P., 2004, *ApJ*, **609**, 589

White R. L., Becker R. H., Helfand D. J., Gregg M. D., 1997, *ApJ*, **475**, 479

Whiting M. T., Webster R. L., Francis P. J., 2001, *MNRAS*, **323**, 718

Wright E. L., et al., 2010, *AJ*, **140**, 1868

Yan T., Stocke J. T., Darling J., Momjian E., Sharma S., Kanekar N., 2016, *AJ*, **151**, 74

York D. G., et al., 2000, *ApJ*, **120**, 1579

Zhu G., Ménard B., 2013, [ApJ, 770, 130](#)  
di Serego Alighieri S., Danziger I. J., Morganti R., Tadhunter  
C. N., 1994, [MNRAS, 269, 998](#)  
van Gorkom J. H., Knapp G. R., Ekers R. D., Ekers D. D., Laing  
R. A., Polk K. S., 1989, [AJ, 97, 708](#)

This paper has been typeset from a  $\text{\TeX}$ / $\text{\LaTeX}$  file prepared by  
the author.